RESEARCH PAPER

CrossMark

Investigation of Arching Effect in Geosynthetic-Reinforced Piled Embankments

Riya Roy[1] · Anjana Bhasi[2] (iD)

Abstract
Column-supported embankments provide a practical and efficient solution for construction on soft soil due to the low cost and short construction times. In recent years, geosynthetics have been used in combination with column systems to support embankments. The load transfer mechanism in these systems is a combination of soil arching and membrane effect of the geosynthetics. In this paper, numerical method was used to improve the understanding of the long-term performance of geosynthetic-reinforced embankments supported on end-bearing piles. The distribution of skin friction, axial force distribution, settlements on the embankment and foundation soil surface, and vertical stresses on the pile head and foundation surface were studied. Finally, the results from the numerical studies were compared with the results from different analytical methods. Based on the numerical results obtained, modified arching coefficient is presented for end-bearing piles.

Keywords Piled embankments · Geosynthetic · Arching · Membrane action · Interaction · Consolidation

1 Introduction

In recent years, due to the advancement in geotechnical techniques and with the help of the latest technology, various ground improvement techniques are used to improve the in situ soil characteristics to suit the foundation of our choice. These techniques help in improving the shear strength and decreasing the compressibility, lateral displacement of soil. For large embankments over deep soft clay deposits, removal of existing soft soil is not practical and the use of low-density soils cannot reduce the loads transferred to the soft ground. When the gain in shear strength and stiffness due to consolidation is unpredictable and availability of land is insufficient to change the embankment geometry, one of the most dependable and convenient solutions among various techniques is the use of column supports to carry the embankment load. Column

supports can be hard columns such as piles or semi-hard columns such as deep cement mixed columns and stone columns (Han and Gabr 2002). The technique consists of a grid of plain concrete piles driven through the soft layer and embedded in a competent substratum beneath, with an embankment above the piles. The conventional pile-supported system requires large pile caps and very closely spaced piles. In the recent years, geosynthetics have been used in combination with piles/column systems to support embankments over soft foundation soils. The application of geosynthetics in the embankment fill just above the piles enhances the load transfer from the soil to columns and reduces the total and differential settlements (Han and Gabr 2002; Liu et al. 2007; Jenck et al. 2009; Van Eekelen et al. 2011; Anjana and Rajagopal 2013, 2015). A single layer of reinforcement is assumed to act as a tensioned membrane (catenary) under the vertical load enabling the deflected basal reinforcement to be analyzed as a parabola (Collin et al. 2005). The load transfer mechanism in these systems is a combination of soil arching and the membrane effect of the geosynthetic. The tensile strength of geosynthetic depends on the portion of the embankment load that is transferred directly to piles due to soil arching. To construct effective and efficient piled embankments, design

✉ Anjana Bhasi
anjanabhasi@nitc.ac.in; anjanabhasi@yahoo.com

[1] Department of Civil Engineering, Chaitanya Bharathi Institute of Technology [CBIT], Hyderabad, India

[2] Department of Civil Engineering, National Institute of Technology Calicut, Kozhikode, Kerala, India

guidelines are required. Several guidelines for geosynthetic-reinforced piled embankment exist (BS8006-1 2010; EBGEO 2011; CUR 226 2010). As these design methods were developed based on different soil arching theories (Terzaghi 1943; Guido et al. 1987; Hewlett and Randolph 1988), the results obtained are not consistent (Smith and Filz 2007).

In this paper, stress–pore pressure coupled analyses were carried out to investigate the time-dependent long-term behavior of GRPS embankments using axisymmetric unit cell models. For practical reasons, unit cell approach is usually adopted to analyze the performance of geosynthetic-reinforced pile-supported (GRPS) embankments. Two-dimensional axisymmetric analysis is carried out since full three-dimensional analyses require high computer memory and analyses time. Even though the two-dimensional finite element models cannot completely represent the realistic conditions, it can give a sufficiently accurate result (Yoo and Kim 2009; Anjana and Rajagopal 2015).

Liu et al. (2007) described the case history of a GRPS highway embankment in Shanghai, China, and the measured field data were compared with the results from full 3D numerical analyses. The present work is based on this case study, and the time-dependent behavior of GRPS embankment systems under various conditions was investigated under different parameters such as the modulus of the column, tensile stiffness of the geosynthetic and pile center-to-center spacing.

2 Numerical Analyses

The finite element analyses were performed using ABAQUS (SIMULIA 2009) due to its robustness in numerical solution strategy for soil nonlinearity and stress–pore pressure coupled problems. Coupled analysis is based on the generalized consolidation theory of Biot (1941), which extended the Terzaghi's (1923) one-dimensional consolidation theory to three-dimensional conditions. This results in both displacement and pore fluid pressure degrees of freedom at the corner nodes of each element.

2.1 Site Conditions

The numerical models were developed by considering the site conditions reported by Liu et al. (2007). The site is located in northern suburb of Shanghai, China. Figure 1 represents the cross section of the embankment. The soil profile consists of a 1.5-m-thick coarse-grained fill of unit weight 20 kN/m^3 overlying a 2.3-m-thick deposit of silty clay having a unit weight of 20 kN/m^3; this deposit overlies a 10.2-m-thick soft silty clay of unit weight 18 kN/m^3.

Underneath the soft silty clay, there is a 2-m-thick medium silty clay which is followed by 9-m-thick sandy silt. The ground water table is at a depth of 1.5 m. The height of the embankment is 5.6 m, and it spans 120 m in the direction perpendicular to its cross section. The crest width of the embankment is 35.2 m, and the side slopes are 1:1.5 (V/H). The embankment is supported by cast in situ concrete piles having external diameter (a) of 1 m and an embedded length of 16 m. Piles are arranged in a square pattern with a pile center-to-center spacing (s) of 3 m. The geosynthetic layer is sandwiched between two gravel layers, each of 0.25 m thickness. The embankment is constructed on the top of the gravel bed over a period of 55 days in nine lifts.

2.2 Methodology

In the first step of the analyses, geostatic command was invoked to establish the initial in situ stresses in the foundation soil. All the pile elements and embankment elements were removed at this stage. Once the geostatic equilibrium (entire model, $U_1 = U_2 = 0$) was established, pile elements were added and interaction was defined along the length of pile and at the top and bottom of pile, where it is in contact with soil. Layers of elements representing the reinforcement–gravel layer (0.5 m) were then added in a single step. Once the reinforcement layer was placed, interaction was activated along the reinforcement–gravel interface. Embankment fill (5.1 m) above the reinforced bearing layer was added in the next eight steps. Consolidation analysis was carried out in each of the steps resulting in settlements as soon as the reinforced bearing layer was placed. The total height of the embankment (5.6 m) was reached over a period of 55 days. After full placement of the embankment layers, consolidation analysis was carried out until the excess pore water pressure fell below a specified near zero value in the soil layer near and at the pile base level.

2.3 Material Models and Parameters

In the present study, four different materials were involved: foundation soil, embankment fill, pile and geosynthetic. The pile was modeled as an isotropic linear elastic material with a Young's modulus of 20 GPa and a Poisson's ratio of 0.2. The geogrid was modeled as an isotropic linear elastic material with a tensile stiffness of 1180 kN/m and a Poisson's ratio of 0.3. The embankment fill, gravel and the surface coarse-grained fill were modeled using a linear elastic–perfectly plastic model with Mohr–Coulomb failure criterion (Table 1). The four foundation soils were modeled as modified cam-clay materials, and the properties are given in Table 2.

Fig. 1 Cross section of the embankment considered in the study based on Liu et al. (2007)
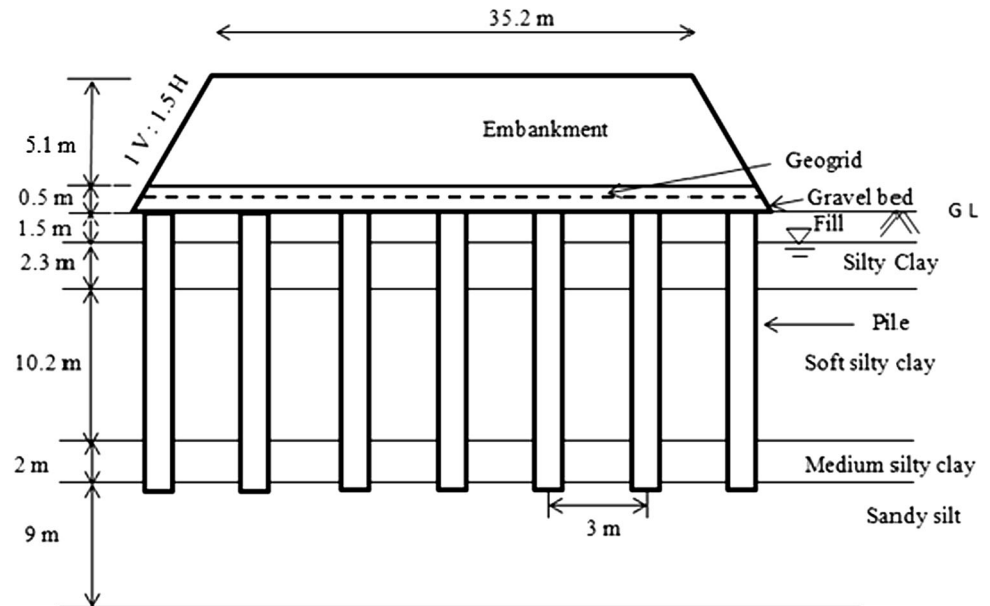

Table 1 Mohr Coulomb material model properties

Material	Cohesion, c' (kPa)	Angle of internal friction, Φ' (°)	Dilatancy angle, Ψ (°)	Young's modulus, (MPa)	Poisson's ratio, μ
Embankment	10	30	0	20	0.3
Gravel	10	40	0	20	0.3
Coarse-grained fill	15	28	0	7	0.3

Table 2 Modified Cam-clay material model properties

Material	μ	λ	κ	M	e_1	$k_w \times 10^{-4}$ (m/day)
Silty clay	0.35	0.06	0.012	1.20	0.87	8.64
Soft silty clay	0.40	0.15	0.030	0.95	1.79	4.32
Medium silty clay	0.35	0.05	0.010	1.10	0.88	4.32
Sandy silt	0.35	0.03	0.005	0.28	0.97	43.2

λ slope of the virgin consolidation line, κ slope of the swelling line, M slope of the critical state line, e_1 void ratio at unit pressure, k_w coefficient of permeability

2.4 Boundary Conditions and Elements Used

A displacement/rotation boundary condition was applied at the bottom and side of the numerical model to constrain the movement of the selected degrees of freedom to zero or to prescribe the displacement or rotation for each selected degree of freedom. At the bottom of the finite element mesh, fixed boundary condition is applied which implies the displacement in all the directions is set to zero ($U_1 = U_2 = 0$). Since the analysis had been done to only half of the unit cell, the model was considered symmetrical about the y-axis (about a plane $X = a$ constant). Hence, the left side of the model is applied with symmetrical boundary condition XSYMM in which displacement component $U_1 = 0$ and rotation components $UR_1 = UR_2 = 0$. A roller boundary condition is applied at the right side of the model in which the displacement along the X direction is restrained ($U_1 = 0$). Regarding the hydraulic boundary conditions, the water table was assumed to be at a depth of 1.5 m below the ground level and the initial pore pressures prior to the embankment construction were taken as hydrostatic. The bottom of the finite element mesh was defined as impermeable, and lateral flow was not permitted across the boundaries.

The elements used in this analysis were CAX8R (8-noded biquadratic axisymmetric quadrilateral with reduced

integration) for pile and embankment fill, CAX8RP (8-noded axisymmetric quadrilateral, biquadratic displacement, bilinear pore pressure, reduced integration) for foundation soil and MAX2 (3-node quadratic axisymmetric membrane) for geosynthetic.

2.5 Interaction

Contact in ABAQUS requires defining pairs of interacting surfaces called contact pairs—master and slave surfaces. The stiffer material is considered as the master surface (e.g., pile when pile–soil interaction is considered), and the flexible material in the pair is termed as the slave surface (e.g., geogrid when geogrid–gravel interaction is considered). Slave nodes should not penetrate master surface segments, whereas the nodes on the master surface can penetrate slave surface segments (Fig. 2). In the present study, pile–soil interaction and geogrid cushion layer interactions are considered. Once the contact pairs have been defined, appropriate contact property is chosen to define the interactions in the normal and tangential directions. (1) *Pile–soil interaction:* In the normal direction, the interface contact was assumed to be hard contact and no separation was allowed (Leng and Gabr 2005). In the tangential direction, Coulomb friction model was used to simulate the interaction, wherein the frictional behavior is specified by an interface friction coefficient (μ) and a limiting displacement. For the present study, limiting displacement of 5 mm was considered based on the findings by Lee et al. (2002). The interface friction coefficient (μ) was calculated from $\tan\delta$ where δ (friction angle between the soil and pile) $= \frac{3}{4}\varphi$ (internal friction angle of soil). (2) *Reinforcement–fill interaction:* Membrane action of the reinforcement depends on the interaction between the reinforcement and the embankment fill material. In the normal direction, the interface contact was assumed to be hard contact and no separation was allowed. In the tangential direction, Mohr–Coulomb failure criterion was used
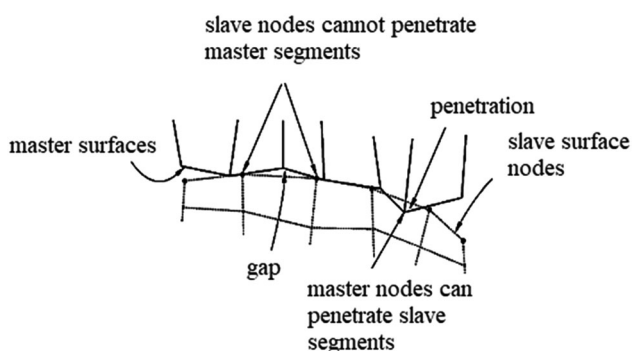
to determine the critical shear stress at interface. Cohesion was considered as zero, and the friction angle at the interface was taken equal to the friction angle of the gravel, for the calculation of critical shear stress (Liu et al. 2007).

2.6 Validation of the Interaction Model Adopted in Present Study

The axisymmetric model adopted was able to predict the settlements and stresses reasonably close to the field measurements reported by Liu et al. (2007) for 125 days after the completion of the embankment (Anjana and Rajagopal 2015). Load transfer mechanism in geosynthetic-reinforced piled embankments is a function of complex soil–structure interaction between the reinforcement, foundation soil and the pile. To account for this behavior, interaction between pile and foundation soil, and reinforcement and coarse-grained fill is considered in this study. The interaction model adopted was validated with the skin friction study carried out by Yao et al. (2012). They presented the study of negative skin friction developed along a super-long pile caused by the soil settlements under large-scale surcharge loading. Numerical results (Fig. 3) based on the interaction model adopted in the presented study showed good agreement with the analytical and measured data given in Yao et al. (2012).

3 Results and Discussion

In geosynthetic-reinforced piled embankments, the load from the embankment is transferred by soil arching and geosynthetic tension. The amount of load transferred to the pile, foundation soil and geosynthetic is studied by
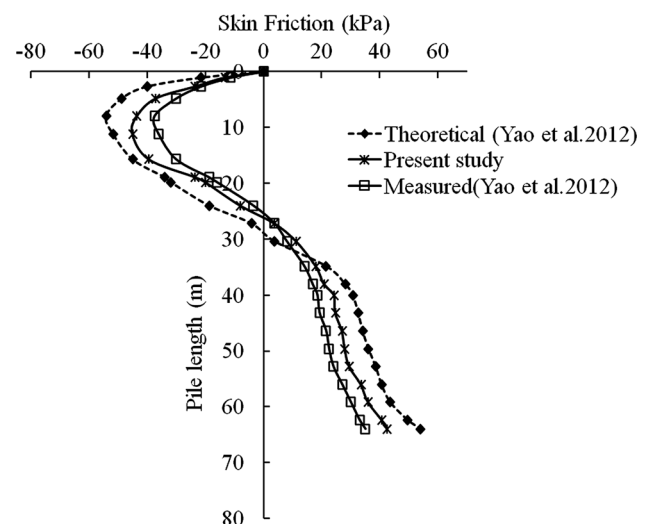

Fig. 2 Contact pairs—master and slave surface (SIMULIA 2009-ABAQUS)

Fig. 3 Validation of the negative skin friction based on Yao et al. (2012)

changing various parameters. Studies were carried out for both reinforced and unreinforced piled embankments with commonly adopted pile spacings of 2.5 m, 3.0 m and 3.5 m. All the parameters were studied with respect to the two critical time periods: (a) end of construction and (b) end of consolidation. Settlement studies showed that consolidation settlements started immediately after the placement of the first layer of embankment soil. During the sequential construction of the embankment in layers, excess pore water pressures were generated within the foundation soil. Consolidation analysis was carried out till the excess pore pressure reduced to near zero in the soil at the pile base level. Figure 4 shows the change in excess pore pressure with respect to time from the numerical analyses. Based on the plot, in all the analyses, 650 days was taken as the time for end of consolidation.

3.1 Load Transferred to the Pile

Majority of the embankment load in GRPS embankments is transferred to the piles due to the soil arching effect. The stiffness of the foundation soil is much lower than the stiffness of the piles. Due to this stiffness difference, the vertical stress from the embankment fill is concentrated onto the piles. Numerically, this phenomenon is investigated by calculating the term stress concentration ratio.

3.1.1 Stress Concentration Ratio (SCR)

The degree of load transfer due to the stiffness difference between pile and soil is quantified by an index called stress concentration ratio (Han and Gabr 2002). It is considered as the ratio of average vertical stress on pile head to the average vertical stress acting on foundation soil. When the stress concentration ratio is high, it indicates that more embankment load is transferred to the piles. The variation
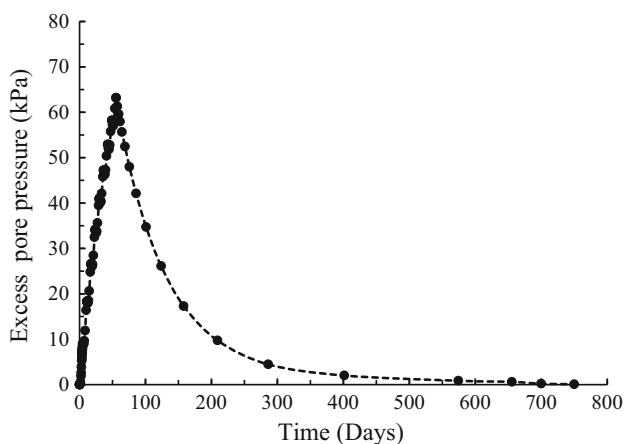
of stress concentration ratio with height of embankment (Fig. 5), pile modulus (Fig. 6) and stiffness of geosynthetic (Fig. 7) is studied for the commonly adopted pile spacings in the field (s = 2.5 m, 3.0 m and 3.5 m). The reinforcement enhances the stiffness of the geosynthetic–soil platform, and less soil arching is developed (Han and Gabr 2002). The unarched vertical stress between the piles is taken by the reinforcement portion between the stiff piles. A single layer of reinforcement acts like a tensioned membrane (catenary), and the load applied normal to the surface of the reinforcement creates tension in the membrane. A portion of the load is transferred to the piles through the vertical component of the tensile forces in the membrane. This membrane effect makes the stress concentration ratio for the reinforced case higher than that for the unreinforced case.

As the embankment height increases, SCR increases and the variation in SCR value becomes less after a particular height of embankment for reinforced (R) and unreinforced (U) case. This further proves that at a particular height from the embankment base, the settlements above the pile and the subsoil surface will be approximately the same which are called the plane of equal settlement. As a result, the differential settlement is reduced with increase in

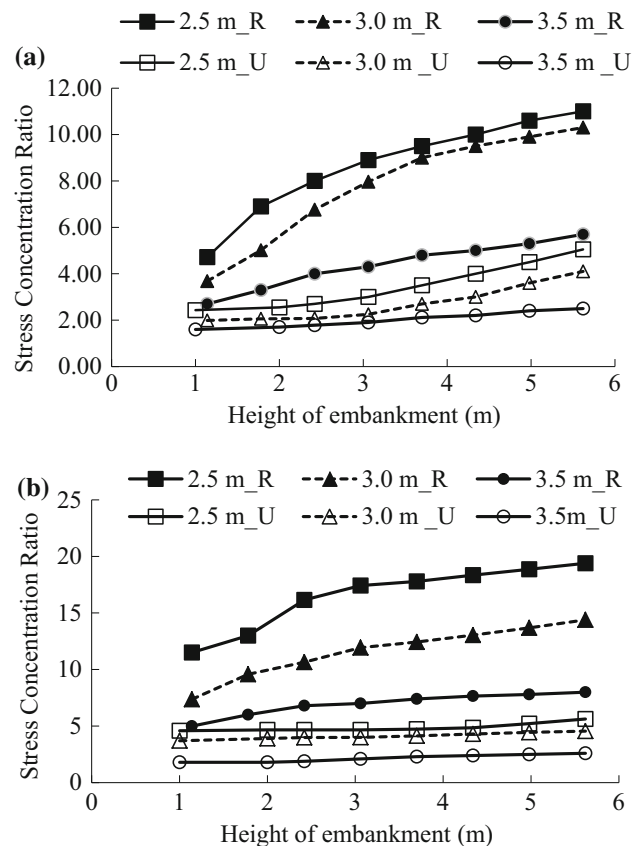Fig. 4 Time history of excess pore pressure in the soil at the pile base level

Fig. 5 Influence of embankment height on SCR **a** end of construction; **b** end of consolidation

Fig. 6 Influence of pile modulus on SCR on SCR **a** end of construction; **b** end of consolidation
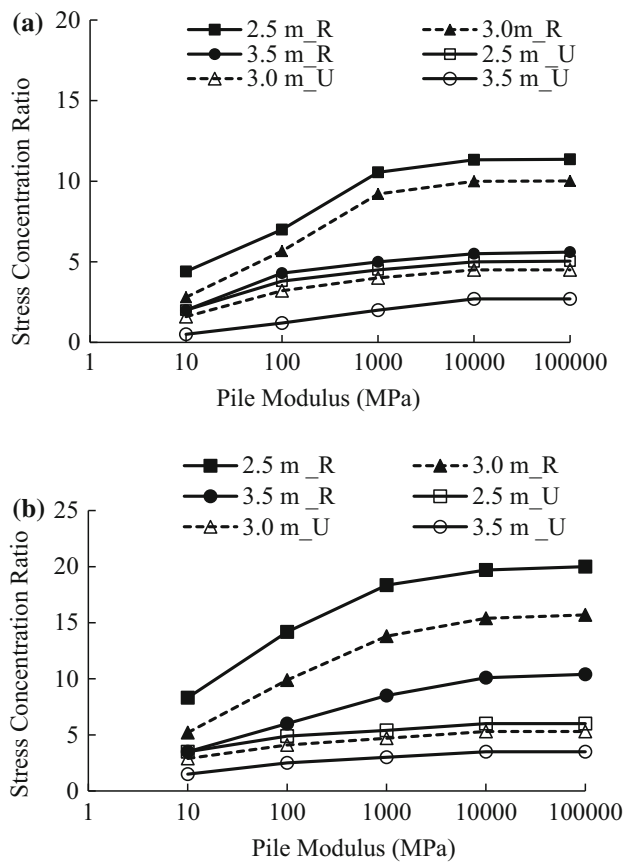

Fig. 7 Influence of geosynthetic stiffness on SCR **a** end of construction; **b** end of consolidation

embankment height beyond full arching height and less soil arching is developed. However, the load transferred to the pile is increased with reinforcement, due to the membrane action of the reinforcement. A large pile center-to-center spacing of 3.5 m in field is economical, but it is not able to aid in the development of arches which considerably reduces the embankment weight transferred to piles due to the arching effect (Fig. 5). SCR is found to increase with an increase in pile modulus (Fig. 6). A higher stiffness of pile increases the differential settlement between the stiffer pile and the soft foundation soil, promoting more load transfer to piles by the formation of arches. When the embankment is reinforced with geosynthetic, the presence of reinforcement will enhance the stress transfer from embankment fill to the piles. This is indicated in the graph showing the variation of stress concentration ratio with stiffness of geosynthetic (Fig. 7). The increase in stress concentration ratio with reinforcement stiffness indicates that the application of reinforcement at the embankment base together with proper pile center-to-center spacing enhances stress transfer from the fill to the piles and this can, in turn, reduce the embankment settlement considerably. For all the cases (Figs. 5–7), SCR increased at the end
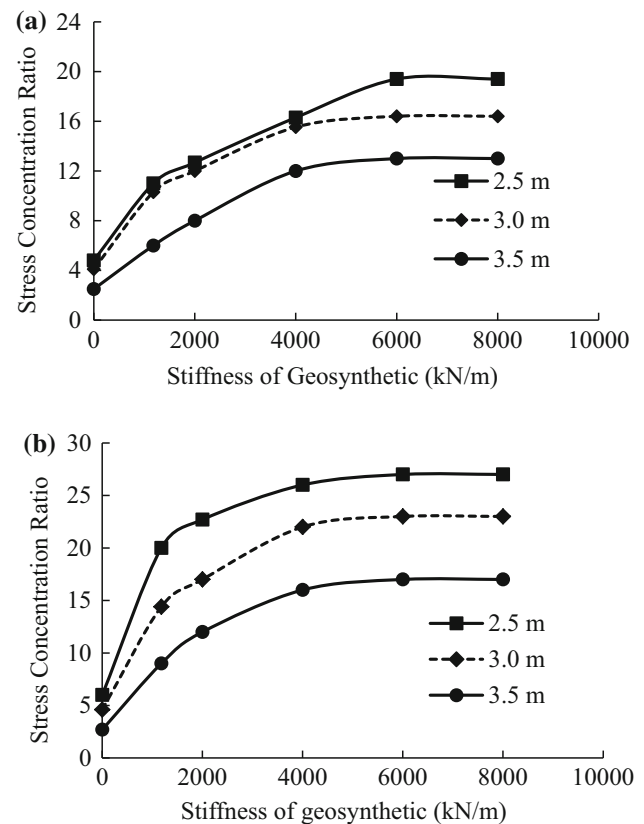
of consolidation. Figure 8 shows the development of arching for geosynthetic-reinforced piled embankment with time (spacing = 3.0 m and reinforcement stiffness = 1180 kN/m). Observation of arches showed that arching action is not an instantaneous phenomenon and the development of arches started during the construction phase and arches were fully developed after some amount of consolidation has taken place. The orientation of principal stresses showed the arch shape as inverted catenary (Fig. 8) as assumed by Hewlett and Randolph (1988).

3.1.2 Soil Arching Ratio or Stress Reduction Ratio

The term soil arching ratio was used by McNulty (1965) to define the degree of soil arching, and it was based on the test results by Terzaghi (1943). Due to the difference in stiffness between the pile and the soft foundation soil, a relative movement occurs between pile and the foundation soil. The downward movement of embankment fill above the soft foundation soil is restrained by the shear resistance developed along the interface in the fill, which reduces the pressure acting on the foundation soil and thereby increasing the load transferred to the piles. This effect is

Fig. 8 Development of soil arching **a** end of embankment construction **b** 20 days after embankment construction **c** 100 days after embankment construction

(a) (b) (c)
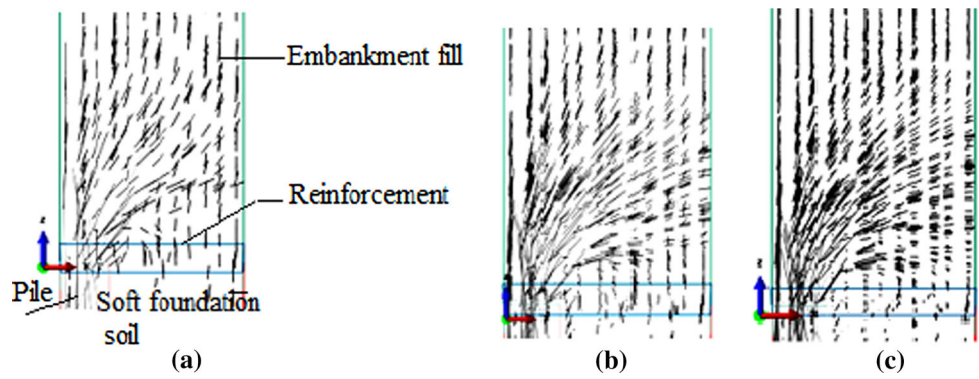
known as soil arching effect, and the degree of this effect is defined as soil arching ratio (ρ) given by:

$$\rho = \frac{p_b}{\gamma H + q_0},\tag{1}$$

where p_b is the applied pressure on the top of the reinforcement, γ is the unit weight of embankment fill, and q_0 is the uniform surcharge on the embankment. If the soil arching ratio is zero, it indicates complete soil arching, and if the ratio is equal to one, it represents no soil arching.

Variation of soil arching ratio with embankment height at different pile center-to-center spacing (2.5 m, 3.0 m and 3.5 m) is shown in Fig. 9. From the results, it is observed that the shear resistance in the fill was not large enough to develop the arching for low embankment height and hence increases the pressure applied on to the reinforcement and foundation soil. With an increase in the embankment height, more shear resistance accumulates which enhances the soil arching mechanism. When reinforcement is provided at embankment base, it stiffens the soft soil layer between the piles reducing the different settlements. Reduced differential settlement hinders the development of arches. As a result, soil arching ratio is greater for the reinforced case than the unreinforced case. The pile stiffness also has great influence on the soil arching ratio. The variation of soil arching ratio with pile modulus is represented in Fig. 10. From Fig. 10, it is observed that the soil arching ratio decreased with an increase in pile modulus for both the reinforced and unreinforced cases up to 10,000 MPa. Increase in pile/column modulus beyond 10,000 MPa had negligible influence on the arching ratio.

The influence of reinforcement stiffness on soil arching ratio is represented in Fig. 11. The stiffness of reinforcement plays a very important role in soil arching. It can be observed that with increase in the reinforcement stiffness, differential settlement in fill reduces and the amount of load transferred to piles due to soil arching reduces. The net effect increases in soil arching ratio. When pile spacing is increased to 3.5 m, effective transfer of shear stress at the embankment fill above the pile is disturbed and arches
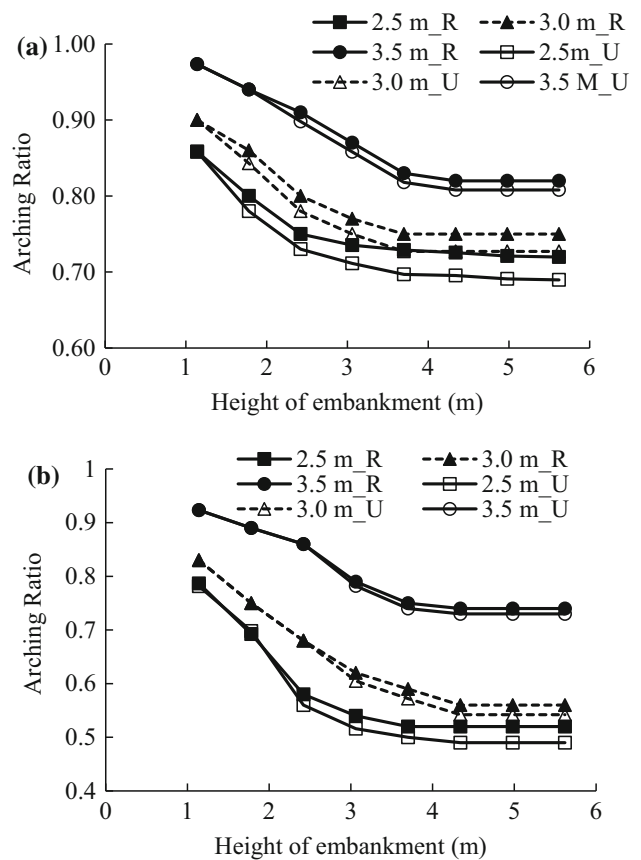

Fig. 9 Influence of height of embankment on arching ratio **a** end of construction; **b** end of consolidation

are not formed. This is evident from the high values of arching ratio for unreinforced as well as reinforced case with different stiffness values. Similar trend is also observed at the end of foundation soil consolidation (Fig. 11a).

3.2 Vertical Stress Acting on the Pile Head and Foundation Soil Surface

Tables 3 and 4 show the variation of vertical stresses acting on the pile head and on the foundation soil surface at the
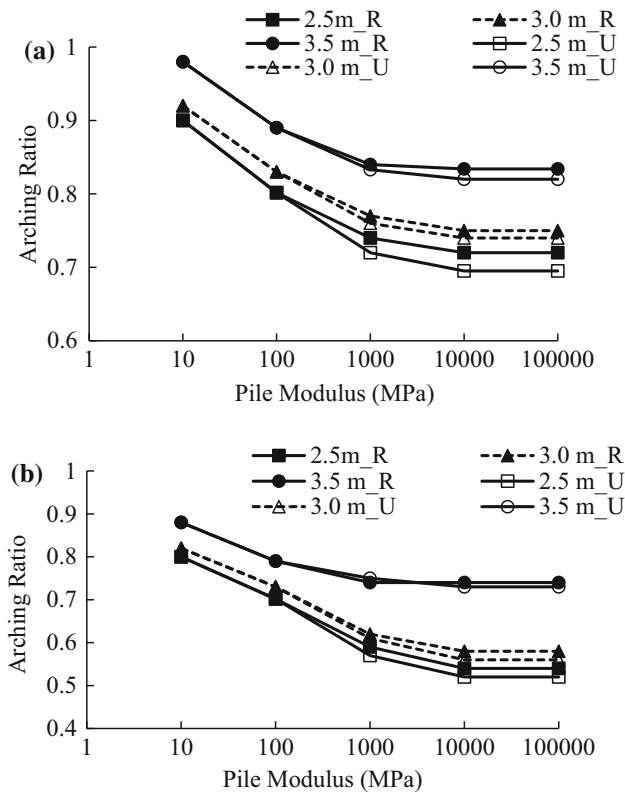
Fig. 10 Influence of pile modulus on arching ratio **a** end of construction; **b** end of consolidation

end of construction of the embankment and at the end of soil consolidation. The vertical stress acting on the pile head and the foundation soil surface increases rapidly during the period of construction, whereas in the consolidation phase, the vertical stresses on the soft soil decreased, while the vertical stress on the pile head increased. This behavior can be explained by the observation in Sect. 3.1.1 that the development of full arching takes place only during the consolidation phase after the construction of embankment. As the pile spacing increases from 2.5 to 3.5 m, the vertical stresses on foundation soil surface are found to considerably increase. This shows that for the load transfer mechanism to fully develop in geosynthetic-reinforced piled embankments, pile center-to-center spacing plays a major role.

3.2.1 Arching Coefficient for End-Bearing Piles from Numerical Analyses

The British Standard BS8006-1 (2010) is the most widely used method for the design of geosynthetic-reinforced piled embankments, and it is very conservative (Van Eekelen et al. 2011). Based on Marston and Anderson (1913) formula for positive projecting conduits, Jones et al. (1990) developed an empirical relationship (Eq. 2) for the
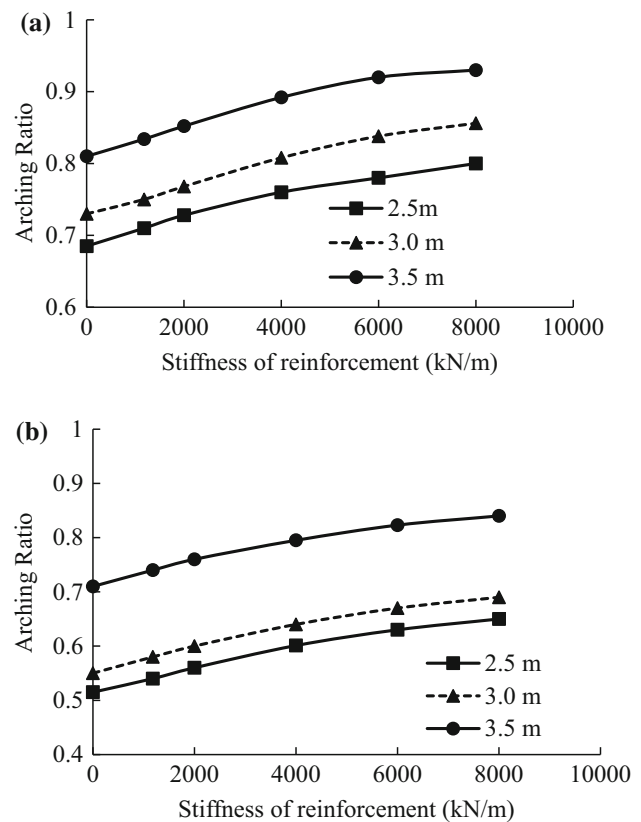

Fig. 11 Influence of reinforcement stiffness on arching ratio **a** end of construction; **b** end of consolidation

ratio of average vertical stress acting on the pile head to the average vertical stress acting across at the base of the embankment.

$$\frac{p'_c}{\sigma'_v} = \left(\frac{a_c a}{H}\right)^2, \tag{2}$$

where p'_c = arched vertical stress per unit length at the top of the conduit/pile, σ'_v = average vertical stress per unit length at the top of the conduit/pile, a_c = arching coefficient (Marston and Anderson 1913), a = pile diameter, and H = embankment height.

BS8006-1 (2010) gives empirical equations for arching coefficient a_c as follows:

$$\text{End bearing piles, } a_c = 1.95\frac{H}{a} - 0.18$$
$$\text{Friction piles, } a_c = 1.5\frac{H}{a} - 0.07. \tag{3}$$

In the present study, concrete pile is resting on a hard sandy silt layer; hence the pile is assumed to be an end-bearing pile. From the numerical analyses, the value for vertical stress acting on the pile head is found for different pile spacings and from Eq. 2 arching coefficient values are calculated. By using curve fitting method, for the range of pile spacing commonly adopted in field ($2 \leq s \geq 3.5$), the

Table 3 Vertical stress acting on pile head for different pile spacing's

Height of embankment (m)	S = 2.5 m		S = 3 m		S = 3.5 m	
	End of construction	End of consolidation	End of construction	End of consolidation	End of construction	End of consolidation
1.1	140.0	148.0	140.0	146.4	100.8	136.7
2.0	211.6	220.9	206.5	215.5	163.6	186.7
2.4	282.0	339.1	267.6	314.9	214.0	269.3
3.1	348.5	395.3	329.1	385.7	249.8	337.0
3.7	413.4	468.9	390.00	461.2	299.5	407.0
4.3	478.4	540.3	452.6	533.1	375.5	509.5
5.0	542.5	608.7	507.2	603.5	465.8	561.6
5.6	607.1	676.4	580.3	674.8	553.8	642.0

Table 4 Vertical stress acting on foundation soil surface for different pile spacings

Height of embankment (m)	S = 2.5 m		S = 3 m		S = 3.5 m	
	End of construction	End of consolidation	End of construction	End of consolidation	End of construction	End of consolidation
1.1	30.7	12.9	36.8	19.9	42	27.3
2.0	31.6	17.0	37.5	22.5	49.6	31.1
2.4	33.4	21.0	39.5	29.6	53.5	39.6
3.1	36.6	22.7	41.3	32.3	58.1	48.1
3.7	40.3	26.4	43.3	37.1	62.4	55.0
4.3	44.0	29.5	47.6	40.9	75.1	66.6
5.0	46.8	32.3	51.2	44.1	87.9	72.0
5.6	50.4	34.9	56.3	46.9	100.7	80.3

following equation is proposed for determining the arching coefficient of end-bearing piles.

$$a_c = m * H^n, \tag{4}$$

where $m = -0.2127*s + 3.2175$ and $n = 0.02015*s + 0.9284$

Pile center-to-center spacing (s) is related to pile diameter (a) with the following equation:

$$a = 1.746e^{-0.222*S}. \tag{5}$$

From Eqs. 4 and 5, arching coefficient depends on embankment height (H), pile center-to-center spacing (s) and diameter/width of piles (a). Numerical studies have shown that pile spacing (s) also plays a major role in load transfer and this parameter is neglected in the equation for arching coefficient in BS8006-1 (2010). Figure 12 shows the variation of arching coefficient with embankment height for different pile spacings using the proposed equation, numerical analyses and BS8006-1 (2010).
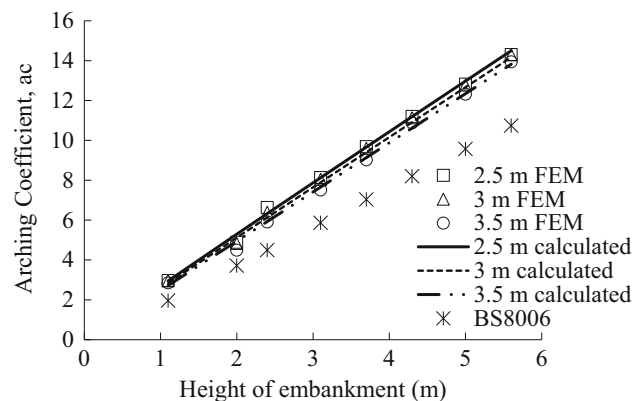
Fig. 12 Comparison of arching coefficient from proposed equation, analyses and BS8006-1 (2010)

Results from the proposed equation are found to be compatible with those obtained from the numerical analyses.

3.3 Load Transfer by Reinforcement

The load transfer mechanism in the GRPS system is the combined effect of soil arching, stress concentration and reinforcement tension. The unarched vertical stress between the piles is assumed to be taken by the horizontal reinforcement. This load applied normal to the surface of the reinforcement creates tension in the polymeric material leading to the membrane effect (Zhan and Yin 2001). The tensile force developed in the reinforcement is transferred to the piles through the vertical component (Han and Gabr 2002).

Numerical analyses help to determine the amount of load transferred by membrane action of the reinforcement to the pile head. The maximum tension developed in the reinforcement from the numerical study for different pile spacings is given in Table 5. In the case of 2.5 m spacing, due to the development of arches, a major portion of the load is taken by the piles. This reduces the load on reinforcement, which in turn reduces the tension developed in the reinforcement. As the pile spacing is increased to 3.0 m, the effect of arching reduces, transferring more load to reinforcement. With further increase in pile spacing to 3.5 m, load transferred to pile is considerably reduced. Also, reinforcement does not take up much load as there is no tensioning in the material which is clear from the tensile force developed in the reinforcement at different time periods (Table 5). Numerical analyses results indicate that for geosynthetic-reinforced piled embankment systems, a pile center-to-center spacing of up to 3d is effective in the development of an efficient load transfer mechanism.

3.4 Negative Skin Friction and Axial Force Study

Studies about stress concentration ratio and soil arching ratio for reinforced and unreinforced piled embankments at different pile spacings showed that the major portion of

embankment weight is transferred to piles through soil arching. Reinforcement tension also helps in transferring a portion of the load to piles. Thus, load-carrying capacity of piles plays a major role in the success of GRPS embankments. According to Cao and Zhao (2012), negative skin friction induced along the pile length influences the settlement of pile and this affects the performance of piled embankments.

From the numerical analyses, negative skin friction values are found with the help of total shear force developed along the axial length on the surface of pile elements. In the study conducted, the entire pile was divided into many sections and axial force along each section was found out. The total shear force corresponding to the local coordinate system at different sections of the pile was obtained, and from these values, the skin friction at each section was calculated by taking the ratio of total shear force to the perimeter of the pile shaft. The skin friction can therefore be calculated as:

$$f_s = \tau/(\pi a l), \tag{6}$$

where f_s is the skin friction at section selected, τ is the total shear force at the section, a is the pile diameter, and l is the depth from pile top to the section.

The total shear force values obtained from the numerical analyses were used to calculate the skin friction values along the pile length. Skin friction values were calculated for different time periods from the end of construction. Figure 13a, b shows the skin friction distribution along the pile length for different pile spacings ($s = 2.5$ m and 3 m based on the observation in Sect. 3.3).

The negative skin friction value decreases as depth increases, and at a point, it changes its sign (positive shaft resistance). The negative skin friction thus obtained can reduce the axial load acting on the piles. The depth at which skin friction value becomes equal to zero which is termed as neutral depth was also determined and is given in Table 6. From Table 6, it is observed that as consolidation

Table 5 Maximum tensile force developed in the reinforcement for different pile spacings

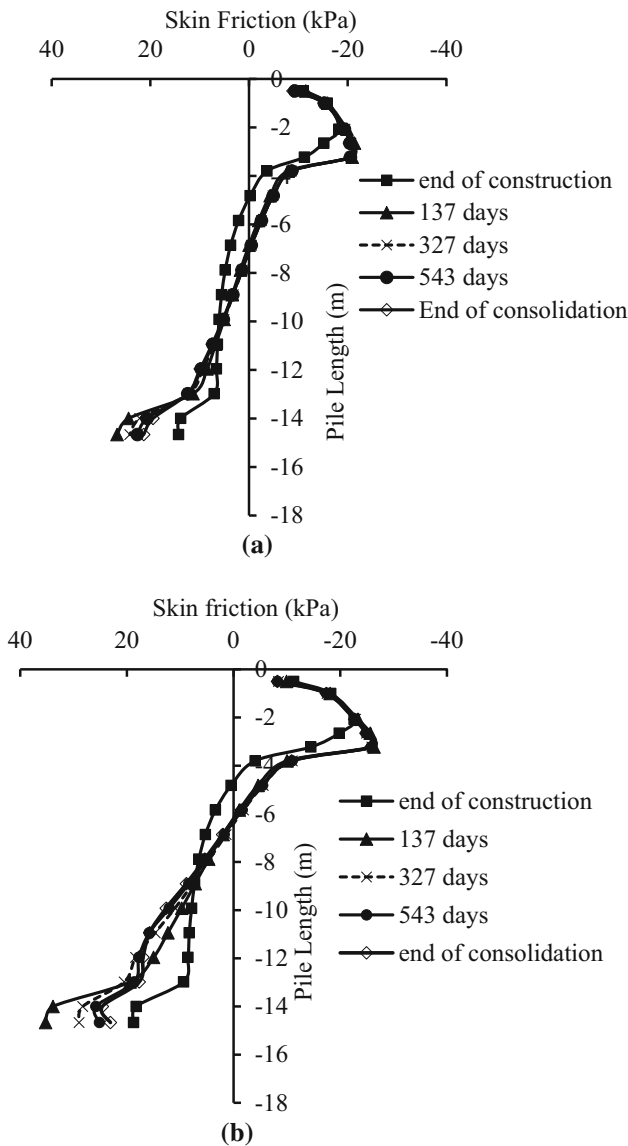| Height of embankment (m)	S = 2.5 m		S = 3 m		S = 3.5 m	
	End of construction	End of consolidation	End of construction	End of consolidation	End of construction	End of consolidation
1.1	1.3	3.1	2.0	10.8	0.6	0.7
1.8	1.9	3.9	2.9	14.0	1.4	1.4
2.4	2.8	5.5	4.0	16.6	1.8	1.9
3.1	3.8	8.5	5.3	18.9	2.0	2.1
3.7	4.9	11.7	6.6	20.8	2.2	2.2
4.3	6.1	14.1	8.2	22.8	2.3	2.4
5.0	7.4	16.4	9.7	24.8	2.5	2.6
5.6	8.7	18.9	11.3	27.0	3.0	3.1

(a)

(b)

Fig. 13 Skin friction variation along pile length for **a** $s = 2.5$ m; **b** $s = 3$ m

Table 6 Neutral depth values for different pile spacings

Time (days)	2.5 m	3 m
55 (end of construction)	5.6	4.7
137	6.8	6.2
327	7.1	6.3
543	7.1	6.4
650 (end of consolidation)	7.1	6.4

proceeds the neutral depth goes on increasing and attains a final value once consolidation is complete.

Along with the skin friction study, axial force distribution along the pile length is also studied. Axial force (P_a) is

calculated by multiplying vertical stress in the pile element with the c/s area of pile at that elevation and is given by:

$$P_a = \text{stress} * \text{area} = \sigma_v \frac{\pi}{4} a^2, \tag{7}$$

where 'σ_v' is the vertical stress in the pile element averaged at an elevation and 'a' is the pile diameter/width at that elevation.

The variation of axial force along the pile length for pile spacings of 2.5 m and 3 m is plotted in Fig. 14a, b.

Along the pile length, the axial force initially increases and after reaching the maximum value it tends to decrease. The initial increase in axial force is due to the negative drag forces developed in the upper sections of the pile where the settlement of the soft foundation soil is more than the settlement of the pile. Axial force is maximum at the neutral plane where the change of negative skin friction to positive skin resistance takes place. Beyond the depth of neutral plane, the axial force in the pile is gradually
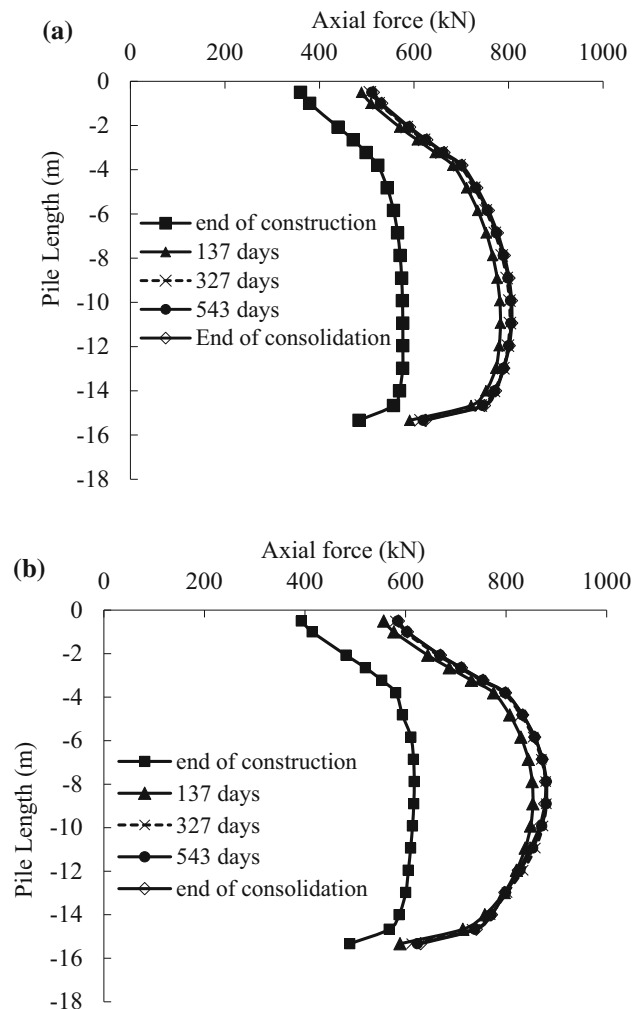
(a)

(b)

Fig. 14 Axial load variation with elevation for **a** $s = 2.5$ m; **b** $s = 3$ m

reduced because of the positive skin friction acting along the surface of the pile. In GRPS embankments, due to the formation of soil arches in the embankment fill, more load is transferred to the piles reducing the negative skin friction. Depth of neutral plane from the pile head decreases when the pile center-to-center spacing is increased to 3 m as more load transfer to pile takes place and positive skin friction starts to develop along the pile length.

3.5 Comparison of Various Design Techniques Using Stress Reduction Ratio (S₃D)

Various design methods are available for the design of GRPS embankments. The value of stress reduction ratio obtained from the various empirical methods, BS8006-1 (2010) and the present numerical study are compared. Stress reduction ratio is a parameter introduced by Low et al. (1994), which is defined as the ratio of the average vertical stress carried by reinforcement to the average vertical stress due to embankment fill. The stress reduction ratio is calculated using different design methods (Terzaghi 1943; Guido et al.1987; Hewlett and Randolph 1988; Low et al. 1994; Kempfert et al. 2004; Abusharar et al. 2009; BS8006-1 2010) for different pile center-to-center spacings and embankment heights. Table 7 gives the equations used in different methods for calculating S₃D. Analytical results are compared with the values obtained from numerical analyses.

3.5.1 Comparison of S₃D from Different Design Methods and FE Analyses Based on Pile Spacing

The stress reduction ratio (SRR) obtained from various empirical methods and the present numerical analyses is shown in Fig. 15. Numerical analyses results predicted higher values for stress reduction ratio compared to different empirical methods. Numerical simulations have shown that arching formation is not an instantaneous phenomenon (Sect. 3.1.1). Arching process starts during the construction phase, as consolidation settlement starts immediately after the placement of the first layer of fill. Full development of arches occurs sometime after the completion of embankment construction (Fig. 8). When pile center-to-center spacing is very large (3.5 m and above), arches are not formed properly and this reduced the load transferred by soil arching which in turn increased the SRR. All the empirical methods including BS8006-1 (2010) gives the SRR at the end of embankment construction, and these methods fail to account for the effect of consolidation on arching. This is best accounted for in numerical simulations which make use of Biot's (1941) consolidation theory.

3.5.2 Comparison of S₃D from Different Design Methods and FE Analyses Based on Embankment Height

Figure 16 shows the variation of stress reduction ratio with embankment height. Analytical methods, BS8006-1 (2010) and numerical simulations show that S₃D decreases with an increase in embankment height. As discussed earlier, with an increase in embankment height, the shear resistance in the fill is large enough to develop arching and transfer more embankment load to the pile top. According to BS8006-1 (2010), when the embankment height is more than the critical height of 1.4(s–a), the height of embankment above critical height plays no role in the forces developed in the reinforcement layer as full weight is transferred to the piles. This trend is not shown by numerical simulations. Figure 16 shows that at a height of 4.6 m and 5.6 m, S₃D values from numerical analyses are nearly the same. This shows the existence of plane of equal settlement, which is formed due to same settlements in the embankment fill above the stiff pile and the soft foundation soil surface. The differences in numerical simulations and empirical methods are attributed to reasons already stated in Sect. 3.5.1.

4 Conclusions

In this paper, finite element-based numerical method was used to improve the understanding of the long-term performance of GRPS embankments on end-bearing piles. Parametric studies based on coupled analyses using Biot's (1941) consolidation theory were carried out using axisymmetric models. Reduction in computational time with the use of Axisymmetric models is proven in literature, and also studies have shown that axisymmetric models are able to predict the behavior of GRPS embankments with reasonable accuracy. Detailed pile–soil and reinforcement–gravel interaction was considered in all the analyses. Load transferred by soil arching and membrane action of reinforcement, distribution of negative skin friction and axial force, vertical stresses on the pile head and foundation surface were studied. Based on the numerical simulations, the following conclusions were drawn:

- As the embankment height increased, stress concentration ratio (SCR) which is a measure of the degree of the load transferred to the stiff piles increased due to the development of enough shear stress in the fill which enhanced the soil arching mechanism. Once the height of embankment reached the plane of equal settlement, variation in SCR became less significant for both reinforced and unreinforced cases.

- Numerical simulations indicated that for geosynthetic-reinforced piled embankment systems, a pile center-to-

Table 7 Equations for calculating S_{3D} from different analytical methods

Authors	Stress reduction ratio (S_{3D})
Terzaghi (1943)	$S_{3d} = \dfrac{\left(1 - e^{-\frac{4HaK\tan\varphi'}{s^2-a^2}}\right) \times (s^2 - a^2)}{4HaK\tan\varphi'}$
Guido et al. (1987)	$S_{3d} = \dfrac{s-a}{3\sqrt{2}\times H}$
Hewlett and Randolph (1988)	At the crown
	$S_{3D} = \left(1 - \left(\frac{a}{s}\right)\right)^{2\times(Kp-1)} \times \left(1 - \frac{s\times 2(Kp-1)}{\sqrt{2}H(2Kp-3)} + \frac{(s-a)2(Kp-1)}{\sqrt{2}H(2Kp-3)}\right)$
	At the pile head
	$S_{3D} = \dfrac{1}{\frac{2Kp}{kp+1}\left[\left(1 - \left(\frac{a}{s}\right)^{(1-Kp)} - \left(1-\left(\frac{a}{s}\right)\right)\left(1-\left(\frac{a}{s}Kp\right)\right) + \left(1-\left(\frac{a^2}{s^2}\right)\right)\right)\right]}$
Low et al. (1994)	$S_{3D} = \dfrac{\sigma_s - \left(\frac{tE_s}{D}\right)}{\gamma H}$
Kempfert et al. (2004)	$S_{3D} = \frac{1}{\gamma H}\left\{\lambda 1^x \left(\gamma + \left(\frac{q}{H}\right)\right)\left[H(\lambda 1 + h_g^2\lambda 2)^{-x} + h_g\left(\lambda 1 + \left(\frac{h_g^2\lambda 2}{4}\right)\right)^{-x} - \left(\lambda 1 + h_g^2\lambda 2\right)^{-x}\right]\right\}$
	where
	$h_g = \text{arching height } = s/2 \text{ for } h \geq s/2 \text{ and } h_g = h \text{ for } h < s/2$
	$\chi = \dfrac{a(K_{crit}-1)}{\lambda_2 s}, K_{crit} = \tan^2\left[45° + \dfrac{\phi'_k}{2}\right], \lambda_1 = \dfrac{1}{8}(s-a)^2, \lambda_2 = \dfrac{s^2 + 2a(s-a^2)}{8}$
Abusharar et al. (2009)	$S_{3D} = \dfrac{\sigma_s - \left(\frac{tE_s}{D}\right)}{\gamma H}$
BS8006-1 (2010)	For partial arching, $S_{3D} = \dfrac{1}{(s^2-a^2)}\left[s^2 - a^2\left(\dfrac{Pc}{\gamma H}\right)\right]$
	For full arching, $S_{3D} = \dfrac{1.4}{H(s+a)^1}\left[s^2 - a^2\left(\dfrac{Pc}{\gamma H}\right)\right]$

Here, H is the embankment height, a is the pile diameter/width, s is the pile center-to-center spacing, φ' is the friction angle of embankment fill, K is the coefficient of earth pressure at rest, ϕ'_k is the characteristic value of friction angle of the embankment material, γ is the unit weight of embankment material, p_κ is the characteristic value of live load, σ_s is the vertical stress acting on the foundation soil, t is the maximum vertical displacement of the foundation soil between pile caps, E_s is the elastic modulus of the foundation soil, D is the depth of the foundation soil, and P_c is the arched vertical stress per unit length at the top of the pile
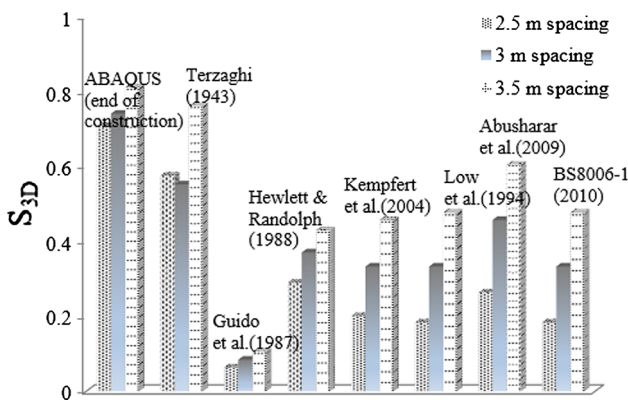

Fig. 15 Variation of S_{3D} with pile center-to-center spacing

Fig. 16 Variation of S_{3D} with height of embankment

center spacing of up to 3d is effective in the development of an efficient load transfer mechanism. A large pile center-to-center spacing in field was economical, but large spacing of piles was not able to aid in the development of arches which reduced considerably the embankment weight transferred to piles due to the arching effect.
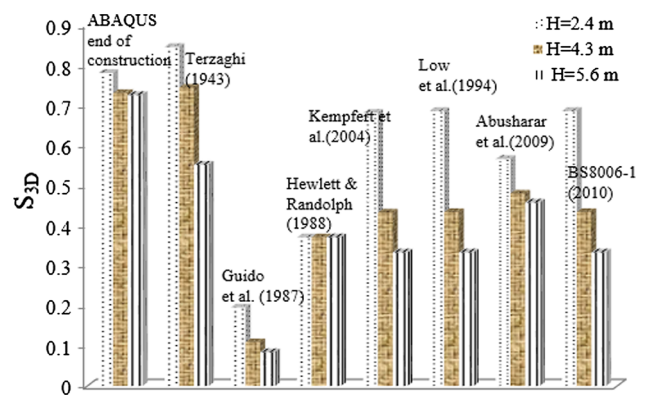
- Studies at the end of embankment construction as well as at the end of foundation soil consolidation indicated that the stress on pile head was more than that on the foundation soil for reinforced as well as for unreinforced embankment. This indicated that a larger portion of the embankment load was transferred to the piles by soil arching which forms the main component in the load transfer mechanism in GRPS.

- As most of the embankment load is taken by piles, time-dependent development and distribution of negative skin friction and axial force along the pile length are very important. Skin friction distribution depends on the correct simulation of interaction effect between pile and surrounding soil. Interaction studies showed that the negative skin friction value decreased as the depth from pile head increased and at neutral plane, skin friction values reduced to zero. After the neutral plane, positive shaft resistance developed as the pile settled more than the surrounding soil. Axial force was maximum at the neutral plane, and beyond the depth of neutral plane, the axial force in the pile gradually reduced because of the positive shaft resistance acting along the surface of the pile. It was observed that as consolidation proceeded, neutral depth reduced and attained a final value once consolidation completed.

- Arching is a time-dependent phenomenon which started during the construction stage and full arches developed during the foundation soil consolidation after the completion of embankment. Empirical methods failed to account for the effect of consolidation on arching.

- The orientation of principal stresses in the numerical results showed the arch shape as inverted catenary as assumed by Hewlett and Randolph (1988).

- Based on the numerical studies, an equation is proposed for calculating arching coefficient for end-bearing piles, which depends on height of embankment (H), pile diameter/width (a) and pile center-to-center spacing (s).

References

Abusharar SW, Zheng JJ, Chen BG, Yin JH (2009) A simplified method for analysis of a piled embankment reinforced with geosynthetics. Geotext Geomembr 27(1):39–52

Anjana B, Rajagopal K (2013) Numerical investigation of time dependent behavior of geosynthetic reinforced piled embankments. Int J Geotech Eng 7(3):232–240

Anjana B, Rajagopal K (2015) Geosynthetic-reinforced piled embankments: comparison of numerical and analytical methods. Int J Geomech 15(5):04014074-1–04014074-12

Biot MA (1941) General theory of three dimensional consolidations. J Appl Phys 12:155–169

BS8006-1 (2010) Code of practice for strengthened/reinforced soils and other fills. British Standard Institution, London

Cao WP, Zhao M (2012) Performance of floating piles for supporting embankments in soft soils. Appl Mech Mater 105–107:1433–1437

Collin JG, Watson CH, Han J (2005) Column-supported embankment solves time constraint for new road construction. In: ASCE geotechnical special publication (GSP) no. 131, contemporary issues in foundation engineering, ASCE Geo Frontiers, Austin, TX, January 24–26

CUR 226 (2010) Ontwerprichtlijn paalmatrassystemen (Design Guideline Piled Embankments). Stichting CUR, Gouda (**in Dutch**)

EBGEO (2011) Recommendations for Design and Analysis of Earth Structures using Geosynthetic Reinforcements – EBGEO

Guido VA, Knueppel JD, Sweeny MA (1987) Plate loading tests on geogrid-reinforced earth slabs. In: Proceedings of geosynthetics 87 conference, New Orleans, pp 216–225

Han J, Gabr MA (2002) Numerical analysis of geosynthetic-reinforced and pile-supported earth platforms over soft soil. J Geotech Geoenvironmental Eng 128(1):44–53

Hewlett WJ, Randolph MF (1988) Analysis of piled embankments. Ground Eng 21(3):12–18

Jenck O, Daniel D, Richard K (2009) Three-dimensional numerical modeling of a piled embankment. Int J Geomech 9(3):102–112

Jones CJFP, Lawson CR, Ayres DJ (1990) Geotextile reinforced piled embankments. In: Hoedt D (ed) Geotextiles, geomembranes and related products. Balkema, Rotterdam, pp 155–160

Kempfert HG, Gobel C, Alexiew D, Heitz C (2004) German recommendations for soil reinforcement above pile-elements. In: Proceedings of the third European conference on geosynthetics, EUROGeo3, Munich, Germany, pp 279–283

Lee CJ, Bolton MD, Al-Tabbaa A (2002) Numerical modeling of group effects on the distribution of drag loads in pile foundations. Geotechnique 52(5):325–335

Leng J, Gabr MA (2005) Numerical analysis of stress–deformation response in reinforced unpaved road sections. Geosynth Int 12(2):111–119

Liu HL, Charles WW, Fei K (2007) Performance of a geogrid-reinforced and pile-supported highway embankment over soft clays—case study. J Geotech Geoenvironmental Eng ASCE 133(12):1483–1493

Low BK, Tang SK, Choa V (1994) Arching in piled embankments. Electron J Geotech Eng 120(11):1917–1938

Marston A, Anderson AO (1913) The theory of loads on pipes in ditches and tests of cement and clay drain tile and sewer pipe. Bulletin No.3, Iowa State University Engineering Experiment Station, Ames, Iowa

McNulty JW (1965) An experimental study of arching in sand. Tech Report I-674, U.S. Army Engineer Waterways Experiment Station, Corps of Engineers, Vicksburg, Mississippi

SIMULIA (2009) ABAQUS/CAE user's manual. Pawtucket, Rhode Island

Smith M, Filz G (2007) Axisymmetric numerical modelling of a unit cell in geosynthetic-reinforced, column-supported embankments. Geosynth Int 14(1):13–22

Terzaghi K (1923) Die berechnung der durshlassijg Jceitsziffer des tones aus dem verlaufder hydrodynamischen spannungserscheinungen (The calculation of the coefficieng of permeability of clays on the basis of hydrodynamic stress phenomena). Sitzungsberichte der Wiener Akademie der Wissenschaften (Mathematisch naturwissenschaftliche Klasse) 132:125–138

Terzaghi K (1943) Theoretical soil mechanics. Wiley, New York

Van Eekelen SJM, Bezuijen A, Van Tol AF (2011) Analysis and modification of the British Standard BS8006 for the design of piled embankments. Geotext Geomembr 29:345–359

Yao W, Liu Y, Chen J (2012) Characteristics of negative skin friction for super-long piles under surcharge loading. Int J Geomech 12(2):90–97

Yoo C, Kim SB (2009) Numerical modeling of geosynthetic encased stone columns. Geosynth Int 16(3):116–126

Zhan C, Yin JH (2001) Elastic analysis of soil-geosynthetic interaction. Geosynthetics Int 8(1):27–48